ECCOMAS Congress 2016
VII European Congress on Computational Methods in Applied Sciences and Engineering
M. Papadrakakis, V. Papadopoulos, G. Stefanou, V. Plevris (eds.)
Crete Island, Greece, 5–10 June 2016

OPTIMIZATION OF A PHOTOACOUSTIC GAS SENSOR USING MULTIFIDELITY RBF METAMODELING

Cédric Durantin[1,2], Justin Rouxel[1], Jean Antoine Désidéri[3] and Alain Glière [1]

[1]Univ. Grenoble Alpes, F-38000 Grenoble, France
CEA, LETI, MINATEC Campus, F-38054 Grenoble, France
e-mail: {cedric.durantin,justin.rouxel,alain.gliere}@cea.fr

[2] University Nice - Sophia Antipolis, 06108 Nice, France

[3] ACUMES Team
INRIA Sophia Antipolis Méditerranée, 06902, Sophia Antipolis,France
e-mail: jean-antoine.desideri@inria.fr

Keywords: Metamodel, Optimization, Multifidelity, Radial Basis Function

Abstract. *The numerical optimization of a photoacoustic gas sensor is a challenging problem in terms of computational time. The signal detected by the gas sensor is a non-linear function depending on several geometrical parameters. The optimization requires a very large number of function calls, thus an important simulation time. In the case of photoacoustics, two different numerical models with different fidelity levels are available to simulate the behavior of the component. In order to reduce the computational burden of optimizing the gas sensor, a new multifidelity metamodeling framework, based on Radial Basis Function, is proposed. The present method offers an alternative to co-kriging (a widely used multifidelity metamodel). This multifidelity model is then used in an optimization sequence to enrich a training database, via a strategy inspired by Gutmann [1]. The process is applied to the optimization of geometrical parameters in the gas sensor problem.*

1 INTRODUCTION

Numerical simulation is widely employed in engineering to study the behavior of future devices and optimize their design. Nevertheless, each computation is often time consuming and, during an optimization sequence, the simulation code is evaluated a large number of times. An interesting way to reduce the computational burden is to resort to a metamodel (or surrogate model) of the simulation code. The process of metamodeling successively implies creating a design of experiment (DOE), evaluating the numerical model response of the DOE and then training the metamodel on the dataset previously obtained. Once the metamodel is built, it can predict the response of the numerical model for a new evaluation point at an extremely reduced time. Thus it can be used in a costly procedure in terms of number of evaluations such as sensibility analysis or optimization. The prediction accuracy depends on the number of points in the dataset and the complexity of the function to replace. Sometimes, models having different levels of fidelity are available and can be hierarchically ranked in accuracy. In this case, multifidelity surrogate modeling aims at efficiently combining information from the different levels of approximation in order to build a metamodel at a reduced cost.

Here the focus is set on the design of a photoacoustic gas sensor. Two different simulation codes are used to describe the performance of the component. The linearized Navier-Stokes equations constitute the high fidelity model and the coarse model consists in the decomposition of the pressure field onto the acoustic modes basis, obtained by solving the homogeneous Helmholtz equation. The computational time for the high fidelity model exceeds one hour on a twenty-core cluster node cadenced at 3 GHz. For the coarse model, the computational time is reported on the same node at 3 minutes. There is a potential time saving in using as much as possible information obtained from the coarse model and still keep good prediction accuracy by also using the expensive model.

Among metamodeling approaches, kriging models [2, 3, 4] are well known in the metamodeling community. This method is attractive because of its capability to estimate a confidence interval of the predicted function. It has recently been revised in order to allow the use of both coarse and complex versions of the computer simulation. This multifidelity approach enhances the prediction accuracy at a reduced computational cost [5]. Then several studies dealing with co-kriging (multifidelity version of kriging) and its use in optimization have been exposed [6, 7, 8]. Radial Basis Functions (RBF) based interpolation method is another existing choice as surrogate model. The new method offers an alternative to co-kriging that might be superior in high dimensional optimization problem, as stated by Regis and Shoemaker on single fidelity problems [9]. To the best of our knowledge, no version of multifidelity RBF-based method has been published at the moment.

The present work offers a new possible way to solve the optimization problem of the photoacoustic gas sensor design via RBF multifidelity metamodeling method (co-RBF). Since some optimization algorithms are already developed for RBF-based optimization [9, 1], they could be extended to a multifidelity version. Here only the so-called Gutmann-RBF method improved by Regis and Shoemaker [9] is used for the multifidelity metamodel based optimization of the gas sensor.

The optimization problem of the photoacoustic gas sensor is described in section 2 and the methodology of the co-RBF metamodeling method is detailed in section 3. The extension of RBF-based optimization algorithm to co-RBF is presented in section 4, together with the result of the gas sensor optimization.

2 MINIATURIZED PHOTOACOUSTIC GAS SENSOR DESIGN

2.1 Physical principle and numerical models

Photoacoustic (PA) spectroscopy is employed to detect gas traces with a high sensitivity, often below the part per billion by volume (ppbv) level. The principle of PA spectroscopy relies on the excitation of a molecule of interest by a light source emitting at the wavelength of an absorption line of the molecule. The light source, usually a laser in the mid-infrared range, is modulated at the acoustic frequency of a resonant cell, containing the gas mixture. During the molecules relaxation, the kinetic energy exchange with the surrounding gas creates local temperature modulation, and thus acoustic waves in the chamber [10].
The cell used in this work is of the differential Helmholtz resonator (DHR) [11] type. It is composed of two chambers linked by two capillaries (Figure 1). The gas excitation is ensured by illuminating one chamber with a laser source. At the Helmholtz resonance of the cavity, acoustic signals in the two chambers are in phase opposition. The signals provided by two microphones measuring the pressure into each chamber are subtracted to provide the PA signal. As the PA signal is inversely proportional to the volume of the resonant cell [10], a trend towards the size reduction of PA cells has been initiated during the last decade [12], [13]. Assuming

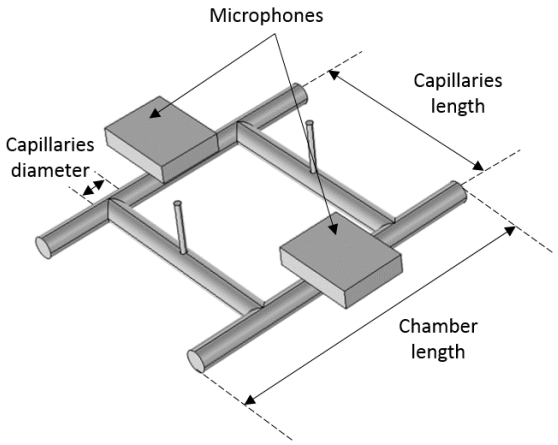

Figure 1: Geometry of a DHR cell.

no viscous and thermal losses and a harmonic heat source, the non-homogeneous Helmholtz equation can be used to compute the pressure field in the cell, and thus the differential PA signal:

$$\nabla^2 p + k^2 p = i\omega \frac{\gamma - 1}{c^2} \mathcal{H} \tag{1}$$

where ω is the modulation frequency, c the speed of sound, γ the Laplace coefficient of the gas, $k = \omega/c$ the wave number and $\mathcal{H}$ the Fourier transform of the power density of the heat source. This pressure acoustic model is computationally efficient and accurate at the macro-scale but fails at the micro-scale. In fact, various volume and surface dissipation processes, at work in the bulk of the propagation medium and close to the walls, cannot be neglected in miniaturized devices, where boundary layers occupy a non-negligible part of the overall cell volume. Numerous approximate models have been adapted from the pressure acoustic model to take into account the dissipation effects. For instance Kreuzer [14], rely on eigenmode expansion of the pressure field and a correction by quality factors. The latter model is fast and faithful enough to

constitute the coarse approximation used in our multifidelity approach.
The rigorous, but CPU time and memory consuming, model relies on the full linearized Navier-Stokes formulation (FLNS), that fully accounts for viscous and thermal dissipation effects. In that approach, small harmonic variations are assumed. The PDE equations system (2) is composed of the continuity equation, incorporating the ideal gas equation of state $p = \rho R_M T$, and the momentum and energy conservation laws:

$$\begin{aligned} i\omega\left(\frac{\tilde{p}}{p_0} - \frac{\tilde{T}}{T_0}\right) + \nabla\cdot\tilde{\mathbf{u}} &= 0 \\ i\omega\rho_0\tilde{\mathbf{u}} = -\nabla\tilde{p} + \nabla\cdot\left(\mu\left(\nabla\tilde{\mathbf{u}} + \nabla\tilde{\mathbf{u}}^T\right) + (\lambda - 2\mu/3)\left(\nabla\cdot\tilde{\mathbf{u}}\right)\mathbf{I}\right) \\ i\omega\rho_0 C_p\tilde{T} = -\nabla\cdot\left(-\kappa\nabla\tilde{T}\right) + i\omega\tilde{p} + Q \end{aligned} \tag{2}$$

where $\tilde{p}$, $\tilde{T}$ and $\tilde{\mathbf{u}}$ are respectively the pressure, temperature and velocity fields of the gas; p_0, T_0 and ρ_0 are the mean values of the pressure, temperature and density fields; λ and μ are the bulk viscosity and the shear viscosity. Q is the heat source.

2.2 Optimization problem

In the framework of the PA sensor case, the FLNS model represents the expensive code and the Kreuzer model the coarse version. The computational time for the FLNS model is actually around one hour and ten minutes on a twenty-core cluster node cadenced at 3 GHz. For the Kreuzer model, the computational time is reported on the same node at 3 minutes. Both models are solved using the commercial software COMSOL (COMSOL AB, Sweden), based on the finite element method.
The PA cell has a chamber diameter of 1 mm and three parameters are involved: chamber length, radius and length of capillaries. Parameters ranges are available in Table 1. The photoacoustic signal detected is the objective to maximize by varying the three geometrical parameters. The new metamodel developed to reduce the computational cost of model evaluations is described in the next section.

Input	Range (mm)
chamber length	[10,20]
capillaries radius	[0.3,0.5]
capillaries length	[5,20]

Table 1: Parameters and ranges of photoacoustic models.

3 MULTIFIDELITY RADIAL BASIS FUNCTION

The basics of RBF-based metamodelling [15, 16, 17, 18] are first briefly explained to introduce the derivation of the co-RBF method. The efficiency of the co-RBF method is not assessed here since it is out of the scope of this paper.

3.1 RBF interpolation model

Given a set of n distinct points $\mathcal{X} = \{\mathbf{x_1}, \ldots, \mathbf{x_n}\}(\mathbf{x_i} \in \mathbb{R}^\mathbf{d}, \mathbf{i} = \mathbf{1}, \ldots, \mathbf{n})$ where the corresponding function values $z_1, \ldots, z_n$ are known, the RBF approximation is defined as a linear combination of the radial basis function φ :

$$\hat{Y}(\mathbf{x}) = \sum_{i=1}^{n} \beta_i \varphi\left(\|\mathbf{x} - \mathbf{x}_i\|\right) + R(\mathbf{x}) \tag{3}$$

Where $\|\cdot\|$ denotes the Euclidean norm in $\mathbb{R}^d$, the coefficients β_i are real numbers and R belongs to the linear space of polynomials in d variables. The radial basis functions used in this paper and the corresponding polynomial forms are given in Table 2. Gaussian RBF gives more freedom to improve the generalization of Equation (3) at the expense of a more complex parameter estimation process. A procedure based on the minimization of the predict error is a possible way to estimate the Gaussian parameter. For a more complete list of available RBF, the reader is referred to Gutmann [1].

RBF	$\varphi(r),\ r>0$	$R(\mathbf{x})$
Cubic	r^3	$\mathbf{a}^T\mathbf{x}+b$
Gaussian	$\exp\left(-\sum_{i=1}^{d}\gamma_i {r_i}^2\right),\ \gamma_i>0$	0

Table 2: Different choices of radial basis functions.

Once a particular φ is selected, the interpolation condition rights:

$$\begin{gathered}\begin{pmatrix}\boldsymbol{\phi} & \mathbf{F}\\ \mathbf{F}^T & 0\end{pmatrix}\begin{pmatrix}\boldsymbol{\beta}\\ \mathbf{a}\\ b\end{pmatrix}=\begin{pmatrix}\mathbf{z}\\ 0\end{pmatrix}\\ \boldsymbol{\phi}_{ij}=\varphi\left(\|\mathbf{x}_i-\mathbf{x}_j\|\right),\ i=1,\dots,n\,,\ j=1,\dots,n\\ \mathbf{F}=\begin{pmatrix}\mathbf{x}_1^T & 1\\ \mathbf{x}_2^T & 1\\ \vdots & \vdots\\ \mathbf{x}_n^T & 1\end{pmatrix}\end{gathered}\tag{4}$$

In the Gaussian RBF case, the system is reduced to $\boldsymbol{\phi}\times\boldsymbol{\beta}=\mathbf{z}$. It can be shown that the system is invertible if and only if the data points are distinct. It is noteworthy that the inversion of this matrix is the most time demanding part of the training of the surrogate model and that, if points in $\mathcal{X}$ are close to each other, the matrix is ill-conditioned. An example of Gaussian and Cubic RBF for the approximation of the modified Branin function [19] is represented on Figure 2, where red dots are the training points and contour lines are the RBF-based metamodel. The training set is constructed with the Latin Hypercube Sampling method [20]. The third plot is the contour of the real Branin function. The Gaussian RBF emulates the Branin function better than the Cubic one because of the parameter $\boldsymbol{\gamma}$ that scales each inputs based on their impact on the output variance.

3.2 Co-RBF

In this work, a multifidelity version of RBF-based metamodel has been developed to solve the photoacoustic gas sensor optimization problem at a reduced computational time. It is now assumed that different levels of modeling in terms of accuracy are available for our physical problem. In the general context, it is possible to link multiple sets of data with different levels of fidelity, but, for sake of readability, the method description is limited here to two datasets. The more accurate set, which is also the more demanding in terms of computational time, is represented by training points $\mathcal{X}_e$ and their corresponding outputs $\mathbf{z}_e$. The coarse simulation model is represented by $\mathcal{X}_c$ and $\mathbf{z}_c$. These training sets can be obtained using the maximin optimized Nested Latin Hypercube designs [21] in order to improve prediction accuracy by better filling the whole input space.

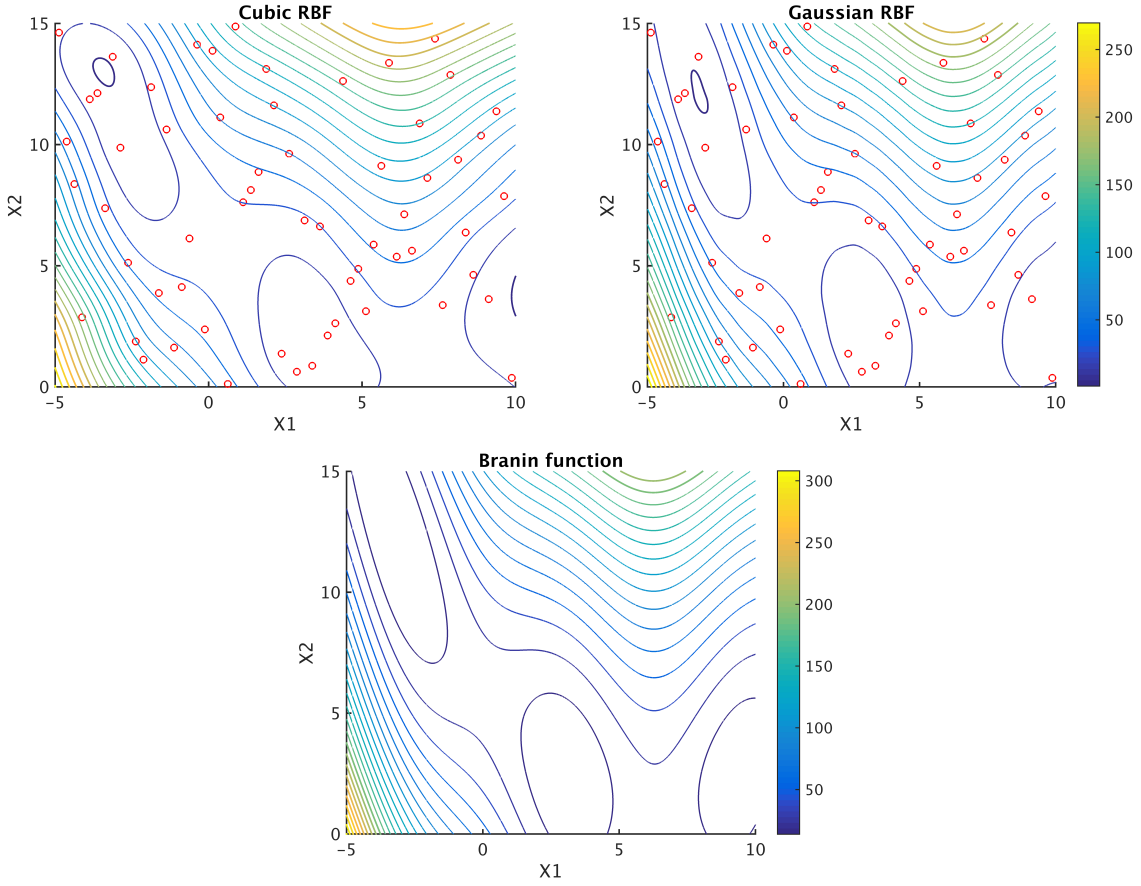

Figure 2: Cubic and Gaussian RBF-based metamodel of the modified Branin function.

The multifidelity approximation is built using the auto-regressive model of Kennedy and O'Hagan [5]:

$$\hat{y}_e(\mathbf{x}) = \rho \hat{y}_c(\mathbf{x}) + \hat{y}_d(\mathbf{x}) \tag{5}$$

where ρ is a scaling factor, y_c the RBF interpolant of the coarse model and y_d the RBF interpolant of the difference between the expensive process and the scaled coarse process. This formulation allows different levels of fidelity to have different correlation structures. The RBF parameters for the coarse and the difference model are not necessarily the same and are estimated separately. To build this multifidelity model, the coarse process is considered independently of the expensive one. Its parameters are estimated within the classical RBF framework described in section 3.1. Once $\begin{pmatrix} \boldsymbol{\beta}_c & \mathbf{a}_c & b_c \end{pmatrix}^T$ obtained, the RBF parameters of the difference function have to be estimated. The assumption is made that, given the point $\mathbf{x}_{c_i}$, no more information can be learnt about $\mathbf{z}_{e_i}$ from the coarse process. This Markov-like property implies that only $y_c(\mathbf{x}_e)$ is considered during the estimation of the difference model parameters. If the dataset $\mathcal{X}_e$ is not evaluated on the coarse model, his corresponding output is predicted by the previously built coarse model RBF. Then the following linear system has to be solved:

$$\begin{pmatrix} \boldsymbol{\phi}_d & \mathbf{F}_e \\ \mathbf{F}_e{}^T & 0 \end{pmatrix} \begin{pmatrix} \boldsymbol{\beta}_d \\ \mathbf{a}_d \\ b_d \end{pmatrix} = \begin{pmatrix} \mathbf{z}_e - \rho y_c(\mathbf{x}_e) \\ 0 \end{pmatrix} \tag{6}$$

The linear system, Equation 6, depends on the unknown scaling factor ρ. Rippa [22] derived a leave-one-out (LOO) formula that estimates the RBF model prediction error. This formula

was initially developed for calibrating the parameter of the Gaussian RBF by minimizing the LOO error. Here this method is used by adding the scaling factor ρ as a parameter to optimize. The LOO formula is given in Equation (7) and its optimization was solved using the covariance matrix adaptation evolution strategy (CMA-ES) [23]. In the Cubic RBF case, the LOO error depends only on the scaling factor:

$$LOO\left(\gamma,\rho\right)=\sum_{i=1}^{n}\left(\frac{\beta_{di}(\gamma)}{\phi_{d_{ii}}^{-1}(\rho)}\right)^{2} \tag{7}$$

An example of the evolution of the LOO depending on γ_d and ρ is available on Figure 3 left, in a test case defined by Forrester et al. [6]. The global minimum of the map is located at $\gamma_d = 1$ and $\rho = 1.74$. This map is obtained from a one-dimensional example displayed on the right plot. Four expensive points and eleven coarse points are evaluated to build the Gaussian co-RBF. The resulting interpolant is the red dashed line and it is close the real model (black solid line).

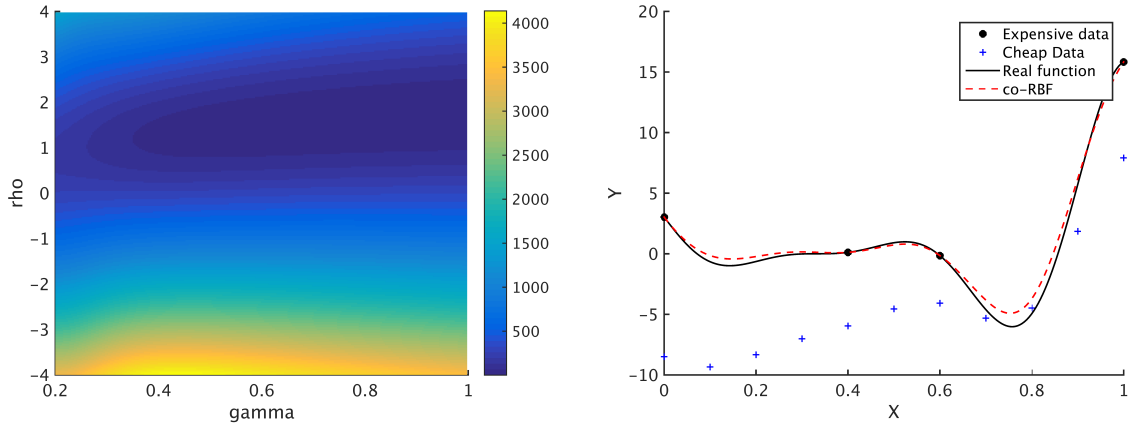

Figure 3: LOO cross-validation error on a one-dimensional example of co-RBF metamodeling.

4 OPTIMIZATION

4.1 Method

An optimization strategy has first been developed by Gutmann [1] in a single fidelity RBF metamodeling approach. It has then been improved by Regis and Shoemaker [9] and referred to as Controlled Gutmann RBF (CG-RBF). This method is an iterative algorithm similar to the Efficient Global Optimization (EGO) procedure derived by Jones [24] for kriging. A design of experiments of the function to optimize is first evaluated and interpolated by a RBF. At each optimization iteration, the RBF interpolant is updated with new evaluated points until the optimum is found. A criterion is defined to select the next infill points based on a measure of the bumpiness of the RBF interpolant [1]. A target value of the global minimum of the function to optimize is cyclically selected to orient the infill criterion toward global exploration or local refinement of the RBF. As a stopping criterion, the maximum number of evaluations is specified by the user.

Some assumptions are needed to transfer the CG-RBF method to the multifidelity framework. First we consider that only the expensive function is called to refine the prediction accuracy in

the vicinity of the global minimum. The evaluation time of the coarse model is considered to be so low that it can be evaluated a large number of time. The prediction accuracy on the coarse model is thus good enough and there is no need to add supplementary training points. Second, since the difference model is built using the expensive points, the infill criterion of the CG-RBF method is computed using the RBF function φ_d. As a result:

$$h_n(l) = \frac{(-1)^{m_\varphi+1}}{[\hat{y}_e(l) - f_n^*]} \times \left[\varphi_d(0) - \begin{pmatrix} u_n^T & F_l^T \end{pmatrix} \begin{pmatrix} \boldsymbol{\phi}_d & F_d \\ F_d{}^T & 0 \end{pmatrix}^{-1} \begin{pmatrix} u_n \\ F_l \end{pmatrix} \right] \tag{8}$$

where $u_n(l) := (\varphi(\|l - x_1\|), \ldots, \varphi(\|l - x_n\|))^T$, $F_l = \begin{bmatrix} l^T & 1 \end{bmatrix}$ and f_n^* corresponds to the targeted minimum value. The optimization of $\min_l - \log h_n(l)$ gives the next infill point.

4.2 Results of the optimization of the photoacoustic gas sensor

The photoacoustic signal detected is the objective to evaluate from simulation models, to surrogate with co-RBF and then to optimize with the CG-RBF-based procedure. The DOE of each model are first defined. For the coarse Kreuzer model, 100 points are evaluated and the RBF built on these data is assumed to be accurate enough. Then 5 points of the expensive FLNS model are evaluated. This allows the training of the co-RBF model in the Gutmann-RBF algorithm extension to multifidelity framework. Our stopping criterion is different from that described by Gutmann [1]. Here it is defined at the end of the target value cycle: once a cycle is over, the optimization stops if a better minimum value has not been evaluated compared to the previous cycle. Five different DOE are tested to check if the optimization leads to the same optimum. The number of evaluations needed to get the minimum location can also be assessed. The obtained results are summarized in Table 3. Two different areas are targeted at the end of the optimization algorithm. Parameters values are close to the upper bounds of the input space. This bound has been set up to fill some integration requirements of the gas sensor in a more complex system. It is either the capillaries length or the capillaries radius that is reduced to get an optimum value around 1.90 Pa. Both solutions provide an improved photoacoustic signal. Note that fabrication uncertainties have not been included yet in the design process but robustness could be a way to select one among the two solutions.

DOE	Optimum location	Optimum value	Number of function calls
1	[20 , 0.5 , 17.7]	1.90	18
2	[20 , 0.5 , 17.7]	1.90	24
3	[20 , 0.47 , 20]	1.90	18
4	[20 , 0.5 , 20]	1.88	12
5	[20 , 0.45 , 20]	1.91	24

Table 3: Results over five initial DOE of the optimization of the photoacoustic gas sensor.

The number of cycles needed to optimize the process is between 2 and 4. Each cycle has a cost of 6 calls to the expensive model. In a previous work, we used only the expensive model with the EGO procedure to get an optimal geometry. The algorithm converged after 40 function calls to a solution with an optimum value of 1.84 Pa and [20 , 0.36 , 19.6] as the optimum location. The benefit of the multifidelity approach developed in this work is clear, in terms of computational time and accuracy of the optimum obtained, when compared to this previous study.

5 CONCLUSIONS

A new multifidelity RBF-based metamodel has been proposed in this work. It is derived through the autoregressive model of Kennedy and O'Hagan [5] and combines the information from the coarse and the expensive numerical model of our design problem. An extension of the CG-RBF optimization algorithm is also suggested in the framework of the co-RBF. This allows the use of a complete multifidelity-based optimization procedure that is an alternative to the co-kriging method combined with EGO.
An optimal design of the photoacoustic gas sensor has been defined by to the new procedure. The extension of the CG-RBF optimization algorithm brings a way to refine the prediction accuracy toward the global optimum of our problem. The results obtained are superior than those obtained with a single fidelity approach in terms of accuracy and computational time.
This work in progress is a first step towards the creation of an efficient co-RBF based optimization algorithm. It has to be supplemented by a complete benchmark between this new procedure and the already existing co-kriging-based optimization method. Furthermore, other extension of already existing RBF-based optimization algorithms, such as the Constrained Optimization using Response Surfaces (CORS) algorithm [9] can be explored. The application of this method to the design of nanophotonic component is also considered.

REFERENCES

[1] H.-M. Gutmann, "A radial basis function method for global optimization," *Journal of Global Optimization*, vol. 19, no. 3, pp. 201–227, 2001.

[2] D. Krige, "A Statistical Approach to Some Basic Mine Valuation Problems on the Witwatersrand," 1951.

[3] C. E. Rasmussen and C. K. I. Williams, *Gaussian processes for machine learning*. Cambridge, Mass.: MIT Press, 2006.

[4] T. J. Santner, B. J. Williams, and W. I. Notz, *The Design and Analysis of Computer Experiments*. 2003.

[5] M. C. Kennedy and A. O'Hagan, "Predicting the Output from a Complex Computer Code When Fast Approximation are Available," *Biometrika*, vol. 87, pp. 1–13, Mar. 2000.

[6] A. I. Forrester, A. Sbester, and A. J. Keane, "Multi-fidelity optimization via surrogate modelling," *Proceedings of the Royal Society A: Mathematical, Physical and Engineering Sciences*, vol. 463, pp. 3251–3269, Dec. 2007.

[7] L. Le Gratiet and C. Cannamela, "Cokriging-based Sequential Design Strategies Using Fast Cross-Validation Techniques For Multi-Fidelity Computer Codes," *Technometrics,*, vol. 57, 2015.

[8] C. S. Reese, A. G. Wilson, M. Hamada, H. F. Martz, and K. J. Ryan, "Integrated Analysis of Computer and Physical Experiments," *Technometrics*, vol. 46, pp. 153–164, May 2004.

[9] R. G. Regis and C. A. Shoemaker, "Constrained global optimization of expensive black box functions using radial basis functions," *Journal of Global Optimization*, vol. 31, no. 1, pp. 153–171, 2005.

[10] A. Mikls, P. Hess, and Z. Bozki, "Application of acoustic resonators in photoacoustic trace gas analysis and metrology," *Review of Scientific Instruments*, vol. 72, pp. 1937–1955, Apr. 2001.

[11] V. Zeninari, V. A. Kapitanov, D. Courtois, and Y. N. Ponomarev, "Design and characteristics of a differential Helmholtz resonant photoacoustic cell for infrared gas detection," *Infrared physics & technology*, vol. 40, no. 1, pp. 1–23, 1999.

[12] R. Bauer, G. Stewart, W. Johnstone, E. Boyd, and M. Lengden, "3d-printed miniature gas cell for photoacoustic spectroscopy of trace gases," *Optics Letters*, vol. 39, pp. 4796–4799, Aug. 2014.

[13] J. Rouxel, J. G. Coutard, S. Gidon, O. Lartigue, S. Nicoletti, B. Parvitte, R. Vallon, V. Zninari, and A. Glire, "Development of a Miniaturized Differential Photoacoustic Gas Sensor," *Procedia Engineering*, vol. 120, pp. 396–399, 2015.

[14] L. B. Kreuzer, "The Physics of Signal Generation and Detection," in *Optoacoustic Spectroscopy and Detection* (Y.-H. PAO, ed.), pp. 1–25, Academic Press, 1977.

[15] M. J. D. Powell, "Radial basis function methods for interpolation to functions of many variables," in *HERCMA*, pp. 2–24, 2001.

[16] M. Buhmann, *Radial Basis Function : Theory and implementattions*. cambridge university press ed., 2003.

[17] N. Dyn, D. Levin, and S. Rippa, "Numerical Procedures for Surface Fitting of Scattered Data by Radial Functions," *SIAM Journal on Scientific and Statistical Computing*, vol. 7, pp. 639–659, Apr. 1986.

[18] R. L. Hardy, "Multiquadric equations of topography and other irregular surfaces," *Journal of Geophysical Research*, vol. 76, no. 8, 1971.

[19] A. I. J. Forrester, A. Sobester, and A. J. Keane, *Engineering design via surrogate modelling a practical guide*. Chichester, West Sussex, England; Hoboken, NJ: J. Wiley, 2008.

[20] M. D. Mckay, R. J. Beckman, and W. J. Conover, "A Comparison of Three Methods for Selecting Values of Input Variables in the Analysis of Output from a Computer Code," *Technometrics*, vol. 42, p. 55, Feb. 2000.

[21] G. Rennen, B. Husslage, E. R. Van Dam, and D. Den Hertog, "Nested maximin Latin hypercube designs," *Structural and Multidisciplinary Optimization*, vol. 41, pp. 371–395, Apr. 2010.

[22] S. Rippa, "An algorithm for selecting a good value for the parameter c in radial basis function interpolation," *Advances in Computational Mathematics*, vol. 11, no. 2-3, pp. 193–210, 1999.

[23] N. Hansen, "The CMA evolution strategy: A tutorial," vol. 29, 2005.

[24] D. R. Jones, M. Schonlau, and W. J. Welch, "Efficient global optimization of expensive black-box functions," *Journal of Global optimization*, vol. 13, no. 4, pp. 455–492, 1998.